DRAFT

Astrometric Observation of MACHO Gravitational Microlensing

A.F. Boden, M. Shao, and J. Van Buren[1]
Jet Propulsion Laboratory, California Institute of Technology, Pasadena, CA 91109

ABSTRACT

This paper discusses the prospects for astrometric observation of MACHO gravitational microlensing events. We derive the expected astrometric observables for a simple microlensing event assuming a dark MACHO, and demonstrate that accurate astrometry can determine the lens mass, distance, and proper motion in a very general fashion. In particular we argue that narrow-angle differential astrometric techniques are sufficient to measure the lens mass, and other lens properties (distance, transverse motion) by applying an independent model for the source distance and motion. We investigate the sensitivity of differential astrometry in determining lens parameters by Monte Carlo methods.

Subject headings: gravitational microlensing, astrometry, dark matter

Introduction

In 1986 Paczyński (Paczyński 1986b) suggested that photometric observations of gravitational microlensing might be used to indirectly study the population of massive compact objects in the galaxy, and in particular MAssive Compact Halo Objects (MACHOs) that might be a significant component of the dark matter thought to exist in the galaxy by dynamical considerations. Paczyński's 1986 paper, and the observational proposals it fostered were met with some skepticism. However, the past several years have seen Paczyński's suggestion spectacularly confirmed – at the time of this writing four separate groups have reported significant numbers of candidate gravitational microlensing events from photometric observations of LMC, SMC, and galactic bulge sources. The large majority of the light curves for these candidate microlensing events match theoretical expectations for single lens objects, and all collaborations report a significant excess of microlensing event candidates above the number expected from known stellar populations. In particular, from their first two years of data the MACHO collaboration reports eight events toward the LMC where only one is expected from known stellar populations, and estimates that roughly

[1]Infrared Processing Analysis Center

half of the ('Xl) ected dark matter in the galactic halo is in the form of dark stellar mass objects such as white dwarfs (Alcock et al 1996). The difficulty in interpreting the MACHO collaboration events is that they are observed photometrically, which does not uniquely determine the mass of the lens instead the MACHO collaboration bases their conclusions on interpreting their event sample observables (amplification, duration) in the context of a halo model (Alcock et al 1996).

Clearly it is desirable to measure MACHO physical properties in a model-free context. This objective has led a number of authors to propose the astrometric observation of MACHO gravitational microlensing events (Høg et al 1995, Miyamoto & Yoshi 1{)95). In particular, Miyamoto and Yoshi proposed the separate astrometric observation of both lensing images in MAC]]() microlensing events (a small misuse of the term microlensing see Paczyński 1 986a), and developed the theory of such astrometry. As we shall argue below, we find this suggestion implausible because of the small separation of the images. Instead, herein we consider astrometry of the lensed center-of-light for dark lenses. We find, as did Miyamoto and Yoshi, that high-precision astrometric observation of such microlensing events allows the estimation of the lens parameters (mass, distance, proper motion) appealing only to the properties of lensing. Moreover, we find the problem of determining a subset the lens parameters (mass, relative parallax, relative proper motion) amenable to narrow-angle differential astrometric techniques similar to those proposed for massive companion search programs. In particular we argue that the lens mass can be directly measured independent of additional assumptions, and the lens distance and transverse velocity can be estimated by appealing to an independent model of source distance and proper motion.

In this paper we assess the ability of astrometry to probe the physical parameters of microlensing events in which the lens is dark. In §2 we introduce the theory to analyze a microlensing encounter as observed by a (near) t('l"l"(%tl'iii] instrument, in terms particularly oriented toward differential astrometry. In §3 we address astrometric sensitivity to microlensing parameters through Monte Carlo techniques. Finally, in §4 we place our results in the context of envisioned astrometric instrumentation, discuss the near term prospects for such an astrometric programs, and mention future extensions to this work.

2. Microlensing Encounter Description

2.1. Instantaneous Theory

As quantitatively described by Refsdal (Refsdal 1964) and recently reviewed by Paczyński (Paczyński 1996a), a gravitational lensing event is photometrically observable when an intervening compact massive object passes close to the line-of-sight to a background source. This phenomenon follows from the curvature of space near a massive object. General Relativity predicts that an object of mass m deflects a light ray by an angle α:

$$\alpha = \frac{4Gm}{c^2 b} \tag{1}$$

where b is the "impact parameter" (transverse separation at the point of closest approach) of the light ray relative to the mass position. In this way the mass acts as an optical lens.

The instantaneous geometry of a background source lensed by an intervening point mass (the lens) is depicted in Figures 1 and 2. When the lens is sufficiently close to the nominal line-of-sight to the background source, an observer (equipped with a telescope of arbitrarily high angular resolution) sees a background disk-like source as two arcs at distinct positions θ_i, corresponding to two solutions of a quadratic equation in the bend angles α_i on opposite sides of the lens. In a plane normal to the unperturbed line-of-sight to the source containing the lens (herein referred to as the transverse lens plane), the apparent positions of the two arcs are at impact parameters b_1 and b_2 relative to the lens, functions of the impact parameter of the unperturbed line-of-sight to the source b_s relative to the lens:

$$
\begin{aligned}
b_1 &= \frac{1}{2}\left(b_s + \sqrt{b_s^2 + 4R_E^2}\right) = \frac{R_E}{2}\left(u + \sqrt{u^2 + 4}\right) \\
b_2 &= \frac{1}{2}\left(-b_s + \sqrt{b_s^2 + 4R_E^2}\right) = \frac{R_E}{2}\left(-u + \sqrt{u^2 + 4}\right)
\end{aligned}
\tag{2}
$$

where all the impact parameters are positive semi-definite quantities, R_E is the so-called Einstein radius:

$$
R_E \equiv \sqrt{\frac{4Gm}{c^2}\frac{D_{sl}D_{lo}}{D_{so}}} = \sqrt{\frac{4Gm}{c^2}D_{so}\,x\,(1-x)}
\tag{3}
$$

and we have introduced a dimensionless impact parameter $u \equiv b_s/R_E$. D_{sl}, D_{lo}, and D_{so} are the source-lens, lens-observer, and source-observer distances, respectively, and x is the fractional separation $x \equiv D_{lo}/D_{so}$. The arcs are labeled image 1 and image 2 in the figures, with image 1 being on the *same* side of the lens as the source. The two images appear separated in the transverse lens plane by:

$$
\Delta b = b_1 + b_2 = \sqrt{b_s^2 + 4R_E^2} = R_E\sqrt{u^2 + 4} \geq 2R_E
\tag{4}
$$

The intensities of the two images can be computed from the fact that any lensing conserves surface brightness. For imperfect lens alignment and constant surface brightness of the source the relative brightness between the arcs and source is given by the ratio of perturbed and unperturbed image Sill'fa("(' areas in the transverse lens plane of Figure 2. The relative intensities (units of the unperturbed source intensity) of the two images are easily shown to be:

$$
\begin{aligned}
A_1 &= \frac{u^2 + 2}{2u\sqrt{u^2 + 4}} + \frac{1}{2} \geq 1 \\
A_2 &= \frac{u^2 + 2}{2u\sqrt{u^2 + 4}} - \frac{1}{2} = A_1 - 1
\end{aligned}
\tag{5}
$$

If we consider lensing of LMC, SMC, or bulge stars by intervening star-like compact masses, then what we observe is limited by the finite resolution of our instrumentation. In particular, for

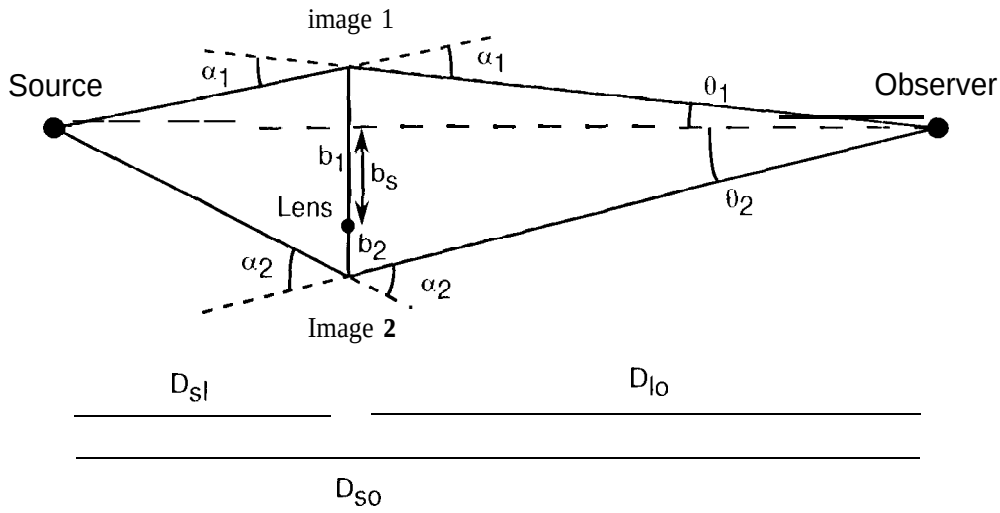

Fig. 1. Lensing geometry in the source-lens- observer plane. Light from the source is perturbed by the presence of the lens and forms two images at the observer locatio n." The light ray bend angles α_i are related to the impact parameters b_i through Eq. 1. The images appear at angles θ_i relative to the nominal source position.

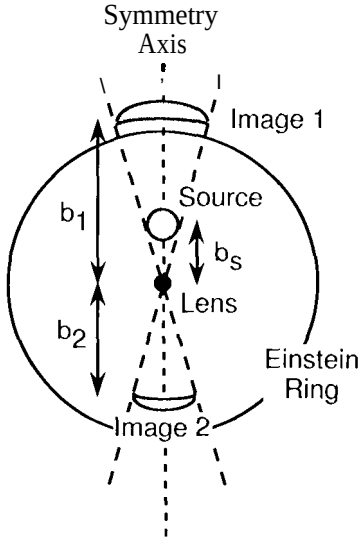

Fig. 2. Lensing geometry normal to the line-of-sight. In a plane normal to the line-of-sight containing the lens, the relative geometry of" the lens, unpert III"I) ('(1 source, and lensed images is shown.

$m \sim M_\odot$ and $D_{lo} \sim D_{so}/2$ ($x \sim 1/2$) we find a value of R_E (hence Δb) that is a few AU. For a lens distance on the order of kilo parsecs, that makes the images separated by an angle on the order of a milliarcsecond (mas 10 "arcseconds). This order of magnitude is well below the angular resolution of available instrumentation, so what is observed is an unresolved source of amplitude (assuming a dark lens):

$$A = A_1 + A_2 = \frac{u^2 + 2}{u\sqrt{u^2 + 4}} \geq 1 \tag{6}$$

The fact that the images are unresolved qualifies this event as *micro*lensing (Paczyński 1986a, Paczyński 1996a). It is important to note that A is significantly greater than one only for u less than one (Figure 3). so the unperturbed source line-of-sight must be within the lens' Einstein radius before significant photometric amplification is observed. Figure 3 gives the image positions and amplitudes as a function of u. Note also that the photometric amplification is purely a geometrical effect, implying it is achromatic a fact that is exploited in photometric microlensing searches.

Center-of-Ligllt Even though the two images are unresolved, they are spatially (list inct from the nominal source position (Eq. 2), and have non-trivial intensities (Eq. 5). We therefore consider the center-of-light position in the instance of microlensing by a dark lens. As can be seen from Figure 2, the center-of-light is clearly on the symmetry axis between the source and lens. Relative to the *lens* position, the center-of-light position $b_{center-lens}$ is straightforwardly obtained from the image positions (Eq. **2)** and intensities (Eq. 5):

$$b_{center-lens} = \frac{A_1 b_1 - A_2 b_2}{A_1 + A_2} = R_E \frac{u(u^2 + 3)}{u^2 + 2}$$

and relative to the *source* position, this center-of-light is located at:

$$\Delta b_{center} = b_{center-lens} - b_s = R_E \frac{u}{u^2 + 2}$$

This center of light position is included in Figure 3 as a function of u. The observable astrometric displacement of the center-of-light from the nominal source position is (Hog et al 1995, Miyamoto & Yoshi 1995, Paczyński 1996b):

$$\Delta\theta(u) = \frac{\Delta b_{center}}{D_{lo}} = \frac{R_E}{D_{lo}} \frac{u}{u^2 + 2} = r_E \frac{u}{u^2 + 2} \tag{7}$$

where we have introduced the angular Einstein radius $r_E \equiv R_E / D_{lo}$. In the microlensing situation described above, $\Delta\theta \sim O(r_E)$ is on the order of a milliarcsecond a value that is within current and envisioned astrometric capabilities of optical interferometers (Palomar Testbed Interferometer PTI (Colavita et al 1994), Keck Interferometer, Space Interferometry Mission SIM (Unwin et al 1997), Global Astrometric Interferometer for Astrophysics GAIA (Lindegren et al 1995)), and even filled-aperture ground-based CCD differential astrometry (Pravdo & Shaklan

1996). It is noteworthy that this astrometric perturbation signature is at a maximum for $u = \sqrt{2}$, and has a value of $2^{-3/2} r_E \approx 0.35\, r_E$. Note also that this perturbation is positive (semi-)definite: the apparent center-of-light is always displaced away from the lens. Finally, as in the case of the photometric amplification, the astrometric displacement is achromatic for our assumption of a dark lens.

2.2. Microlensing Encounter - Barycentric Observer

The geometry of a typical, simple microlensing encounter observed in a barycentric (inertial) system is depicted in Figure 4. The source, lens, and observer are taken as free to move linearly on the time scale of the lensing event. Consequently, viewed in a plane containing the lens and normal to the unperturbed source line-of-sight, the relative source-lens trajectory is approximately linear during the encounter. Without loss of generality we may define a coordinate system in which the source appears stationary and assume that only the lens is in motion. Defining the x-y plane of that coordinate system in the transverse lens plane centered on the source (projection), and taking the x-coordinate along the trajectory of the lens, we can write the lens motion in this system as:

$$\mathbf{x}_{lens}(t) = \begin{Bmatrix} v(t - t_{max}) \\ b_{min} \end{Bmatrix}$$

with v as the relative lens-source transverse speed, b_{min} as the minimum source-lens impact parameter, and t_{max} the time of (transverse) lens-source closest approach or maximum amplification ($b_s = b_{min}$ at $t = t_{max}$). This relative trajectory yields a simple expression for the dimensionless source-lens transverse separation $u(t)$ (and its vectorial counterpart $\mathbf{u}(t)$):

$$u(t) = \frac{\sqrt{b_{min}^2 + v^2(t - t_{max})^2}}{R_E} = \sqrt{p^2 + \frac{(t - t_{max})^2}{t_0^2}} = \sqrt{p^2 + [t]^2}$$

$$\mathbf{u}(t) = \mathbf{x}_{lens}(t)/R_E = \begin{Bmatrix} [t] \\ p \end{Bmatrix} \tag{8}$$

where we have defined dimensionless minimum impact parameter $p \equiv b_{min}/R_E$, the characteristic time or time scale for the microlensing event $t_0 \equiv R_E/v$ the time required for the lens to move transversely one Einstein radius, and a normalized (dimensionless) time coordinate $[t] \equiv (t - t_{max})/t_0$. To predict the time-dependent microlensing observables, $u(t)$ or $u(t)$ (Eq. 8) is inserted into the expressions for the combined image light amplification (Eq. 6) and apparent astrometric perturbation (Eq. 7). Figure 5 gives the relative photometric signature for simple microlensing events in magnitude units for several values of the minimum impact parameter p (p = 0.2, 0.4, 0.6, 0.8, and 1). This light curve shape is precisely the photometric signature for simple microlensing: current microlensing survey projects (OGLE Paczyński et al 1995, MACHO Alcock et al 1996, EROS Renault et al 1996, DUO Alard et al 1995b) first started observing

such lightcurves in 1993, and by this time have observed many such light curves that agree well with this simple theoretical expectation.

Figure 7 gives the plots of the astrometric perturbation signature magnitude as a function of (normalized) time for the p-values given in Figure 5. Note that this perturbation is directed along the instantaneous symmetry axis, which rotates (counterclockwise with increasing time for the geometry in Figure 4) during the microlensing encounter. As seen by the observer the source apparently performs an elliptical excursion from its unperturbed position. The apparent source astrometric excursion is straightforwardly obtained by inserting (the vectorial components of) $u(t)$ (Eq. 8) into $\Delta\theta(u)$ (Eq. 7):

$$\Delta\vec{\theta}([t]) = \frac{R_E}{D_{lo}} \frac{\mathbf{u}([t])}{u^2([t]) + 2} = \frac{r_E}{p^2 + [t]^2 + 2} \begin{Bmatrix} -[t] \\ p \end{Bmatrix} \tag{9}$$

This elliptical excursion is depicted in Figure 6 for our sample values of p from above. It is likewise straightforward to derive the eccentricity of this excursion in terms of p:

$$e = \sqrt{1 - \frac{p^2}{p^2 + 2}} \tag{10}$$

The excursions become more eccentric with decreasing p, as the maximum intensity of the two images is approximately equal (Eq. 5). The maximum magnitude of the astrometric signature, $2^{3/2} r_E$, is the same for all photometrically observable ($p \leq 1$) events — the maximum astrometric perturbation magnitude is the same for all events with $p \leq \sqrt{2}$. The angular Einstein radius is given in Figure 8 as a function of lens distance for bulge and LMC microlensing events and a representative range of lens masses ($m = 0.05, 0.1, 0.25, 0.5, 1\,M_\odot$). For example, a $m = 0.1\,M_\odot$ object at 8 kpc lensing a LMC source has an angular Einstein radius of 3×10^{-1} arcseconds or 300 microarcseconds (1 microarcsecond, abbreviated μas, equals 10^{-6} arcseconds) and a maximum astrometric signature of roughly 100 μas.

It is noteworthy that the time evolution of the astrometric excursion is non-uniform. Far from lens-source closest approach the apparent source motion is slow, while near the closest approach the source motion is significantly higher. This behavior is depicted in Figure 10 (where points are plotted along the excursion trajectory at equal time intervals), and can be seen by differentiating the astrometric excursion with respect to time:

$$\frac{d\,\Delta\vec{\theta}([t])}{d[t]} = \frac{r_E}{(p^2 + [t]^2 + 2)^2} \begin{Bmatrix} p^2 - [t]^2 + 2 \\ 2p[t] \end{Bmatrix} \tag{11}$$

Clearly for $[t]^2 >> p^2$ (i.e. far from maximum amplification) the excursion rate magnitude goes as $[t]^{-2}$. This behavior is significant in that the astrometric excursion described in Eqs. 9 and 11 appears very different than the time-harmonic astrometric excursion expected if the source has massive gravitational companions.

Finally, it is illustrative to compare the time scales for the photometric and astrometric perturbations caused by a microlensing encounter. Figure 9 plots the photometric amplification

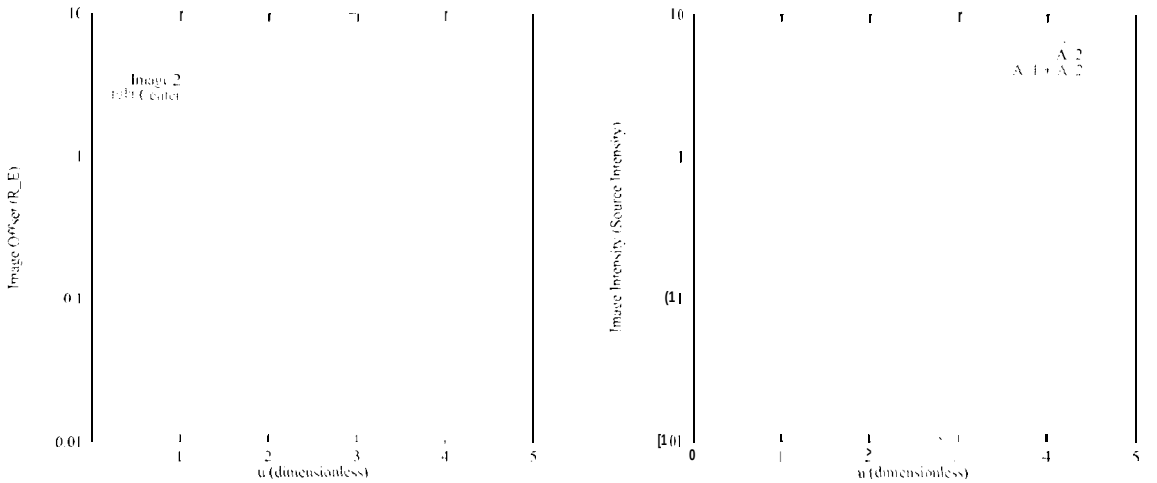

Fig. 3. Image positions and intensities. Left: The two image apparent positions and the center-of-light apparent position (in the transverse lens plane) as a function of u. Right: image (image 1, image 2, combined) intensities (relative units) as a function of u.

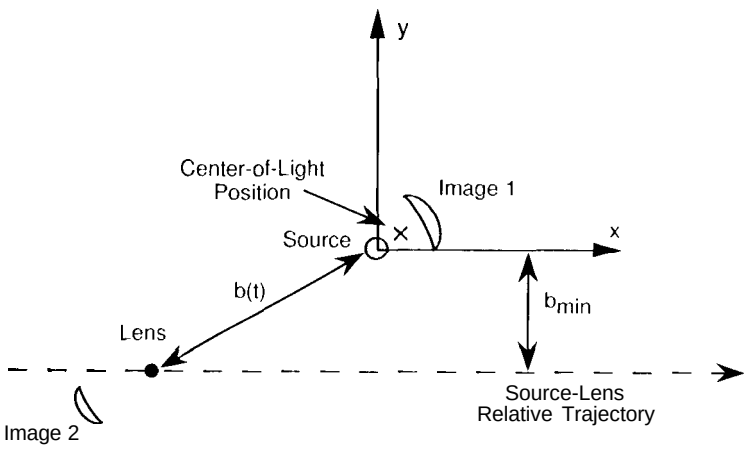

Fig. .4. Microlensing encounter geometry. The geometry of a microlensing event is depicted in a plane normal to the source line-of-sight containing the lens. The relative source-lens trajectory moves from left to right, and is parameterized by the lens speed and minimum impact parameter relative to the source.

and astrometric perturbation magnitude for positive (normalized) encounter times for a $p = 0.4$ microlensing event. The photometric amplification decays from maximum to nominal level in one single time scale (t_0). In sharp contrast, the astrometric effects are much more persistent, roughly requiring factors of 30 and 300 more time to decay to 10% and 1% of the maximum astrometric signature respectively. The MACHO collaboration reports a typical time scale t_0 for a microlensing event to be on the order of one month. Figure 9 makes the point that measurable microlensing astrometric perturbations in events with such a t_0 will span a period of years – depending on the astrometric sensitivity.

The case for astrometric observation of microlensing events is both clear and compelling. Barycentric photometric measurements alone constrain the normalized impact parameter p and time scale t_0 for a microlensing event through Eq. 6 (Figure 5). Astrometric measurements (in lieu of or in addition to photometric measurements) made by a barycentric observer additionally constrain the angular Einstein radius r_E and the lens transverse motion direction (orientation of our x-axis) for the microlensing event through Eq. 9. These two quantities taken together are sufficient to compute the (relative) proper motion of the lens object. However, because the distance to the lens is not directly established, no direct inference can be made about R_E, and thereby the mass and transverse velocity of the lens.

2.3. Microlensing Encounter – Near-Earth Observer

If the microlensing astrometry is observed by an (near) Earth-based instrument over an extended period of time, parallactic effects due to the finite source and lens ranges become important as the assumption of linear relative motion in §2.2 is badly broken by the motion of the observer. Figure 10 depicts an example of astrometric trajectories as viewed by barycentric and terrestrial observers for an arbitrary $p = 0.4$ microlensing event. An LMC source is assumed to be lensed by a 0.1 $M_\odot$ lens at 8 kpc ($r_E \sim 300\mu$as). It is clear that astrometry sufficient to measure the microlensing astrometric excursion will also observe the relative parallactic motions of the source and lens. So unlike the case of barycentric observations, the distance to the lens (actually, the relative source/lens distance) is accessible by this parallax measurement, and a model-independent estimate of the lens mass and (transverse relative) velocity can be derived. An independent model for source distance and proper motion allows the lens distance and motion to be estimated. A clear case of making virtue from necessity.

An observer at barycentric 3-position $\mathbf{b}$ (measured in AU) observes a source in barycentric direction $\hat{\mathbf{n}}_b$ to have an apparent parallactic deflection:

$$\pi\,[\hat{\mathbf{n}}_b(\hat{\mathbf{n}}_b \cdot \mathbf{b}) - \mathbf{b}]$$

with π as the parallax of the source (given in arcseconds by the reciprocal of the distance to the source in parsecs). In the case of microlensing both the source and lens are at finite distance, so both acquire parallactic displacements. In the two-dimensional microlensing coordinate system of

§2.2, we can write the time-dependent correction to the (normalized) source-lens separation $\mathbf{u}(t)$ (Eq. 8):

$$\Delta\mathbf{u}(t) = \frac{\pi_{lens}}{r_E}[\hat{\mathbf{n}}_{lens}(\hat{\mathbf{n}}_{lens}\cdot\mathbf{b}(t))\ \mathbf{b}(t)] - \frac{\pi_{source}}{r_E}[\hat{\mathbf{n}}_{source}(\hat{\mathbf{n}}_{source}\cdot\mathbf{b}(t))\ \mathbf{b}(t)]$$
$$\approx \frac{\pi_{lens}-\pi_{source}}{r_E}[\hat{\mathbf{n}}(\hat{\mathbf{n}}\cdot\mathbf{b}(t))\ \mathbf{b}(t)] = \frac{\Pi}{r_E}[\hat{\mathbf{n}}(\hat{\mathbf{n}}\cdot\mathbf{b}(t))\ \mathbf{b}(t)] \tag{12}$$

assuming $\hat{\mathbf{n}}_{lens}\approx\mathbf{n}_{source}\approx\mathbf{n}$ (($7//71 \sim O(10^{-9})$), defining the relative lens-source parallax $\Pi\equiv\pi_{lens}-\pi_{source}$, and with $\hat{\mathbf{n}}$ and $\mathbf{b}$ rotated into the microlensing coordinate system (so the z component is indeed zero). With this parallactic correction to $\mathbf{u}(t)$, Eq. 9 predicts the astrometric excursion observed by the terrestrial observer (an example of which is depicted in Figure 10). However, it is important to remember that Eq. 9 refers to the excursion *relative* to the unperturbed source position, which itself now appears to move with time due to parallactic effects. This formulation is reasonable, because, as we will argue below, this observational problem lends itself to ground-based narrow-angle differential astrometry techniques.

There are several remarkable points concerning the finite range correction to the microlensing astrometry. First, as noted above, fitting a model based on Eq. 9 to such astrometric data allows the *direct* estimate of all the physical parameters for the lens. Strictly speaking, this statement assumes D_{so} and the source proper motion can be separately established (or inferred) by other means. However, the lens mass is a special case in that it can be estimated just from quantities we observe directly, namely r_E and Π. This fact can be seen by inverting Eq. 3 to solve for m:

$$m = \frac{c^2}{4G}\frac{R_E^2}{D_{so}\,x(1-x)} = \frac{c^2}{4G}\frac{D_{so}r_E^2}{x(1-x)} = \frac{c^2}{4G}\frac{r_E^2}{\Pi}\ [pc] \tag{13}$$

where the last equality comes from the fact that $x/(1-x) = 1/D_{so}\Pi$ with D_{so} in pc and Π in arcseconds. '1'11(! units of r_E are in radians and Π in arcseconds, and the $[pc]$ factor is the length of a parsec expressed in the length units of c and G (('p,.. meters). The dimensions of Eq. 13 are lacking in elegance, but the result is that we have exchanged the uncertainty in D_{so} for the uncertainty in the definition of an astronomical unit. The second interesting point is to note the breaking of the time symmetry around t_{max} by the parallactic correction. Figure 10 demonstrates this point in a particular instance as the barycentric t_{max} time points are labeled on the two excursion trajectories. The degree of symmetry breaking is dictated by the observer's orbit phase and source position in the sky. In general this parallactic symmetry breaking leads to asymmetric lightcurves and different times for maximum amplification for the barycentric and terrestrial observer, both of which have been noted by other authors (Gould 1992, Miyamoto & Yoshi 1995, Buchalter & Kamionkowski 1996, Gould 1996, Gaudi & Gould 1997), and has been observed (Alcock et al 1995).

3. Astrometric observations

During a MACHO microlensing encounter photometric observations alone constrain the impact parameter p and t_0 through Eq. 6, while astrometric observation can be used to uniquely determine the fundamental parameters of the lens (mass, range, and transverse velocity) without appealing to a lens population model. Strictly speaking, computing the lens range and transverse velocity requires the source distance and proper motion to be separately established, while the lens mass can be estimated without appealing to the source distance provided the relative parallax can be established (Eq. 13). For LMC, SMC, and bulge events identified by photometric search programs, assuming ()(10%) distances by source membership in these groups is a plausible situation. Source proper motion relative to a differential astrometric frame can be estimated by astrometry at late encounter times. These conditions imply that the required astrometric measurements can be made differentially against background objects that share common gross parallactic and proper motions with the lensed source. For the dense LMC, SMC, and bulge fields used in photometric searches this approach seems plausible, as the quantity $\delta D/D$ among the reference object S (a natural measure of the scatter in parallax and proper motion) is small for the objects in these fields. These considerations strongly suggest a program to perform differential astrometry on microlensing candidate events detected in photometric surveys.

It is interesting to investigate the sensitivity that such an astrometric program would produce. To address this question we have ("()]1S1 ruct ('(1 a simulation code that creates synthetic photometric and astrometric measurement sets, and then fits a parametric microlensing model to these measurement sets. The code is structured to perform this operation in a Monte Carlo mode, so error distributions in the microlensing parameters may be empirically derived as a function of physical parameters and measurement error. Figure 11 shows sample outputs of the synthetic observation and fitting process for an LMC microlensing event. For this example the lens is again assumed to be at distance of 8 kpc ($\Pi = 100\ \mu$as), $r_E = 300\ \mu$as ($R_E \sim 2.4$ AU, $m \sim 0.1 M_\odot$), $t_0 = ()$.1 yr (relative lens-source transverse speed of 120 km s^{-1}), and a lens motion position angle of 30 deg. Operationally we assume the event is detected photometrically, and an astrometric campaign starts this implies astrometry near and after maximum amplification. Assuming 3% photometry and 1() μas differential astrometry referenced to t 11(1 unlensed source position, we fit a parametric microlensing model to the combined data set The fit is seen to reproduce the measurement sets faithfully, and predicts the microlensing parameters accurately. Figure 12 shows the microlensing parameter residuals obtained in 500 instances of the event depicted in Figure 11. In particular, we observe 2% and 1 6% fractional sample standard deviations on the r_E and Π residual distributions respectively. (Fitting Gaussian profiles to the central parts of the residual distributions result in error estimates that are $\sim 20\%$ better that the sample standard deviations). Using the sample standard deviation figures, the error in estimating the lens mass is 1 6% in Eq. 13, clearly dominated by the parallax error.

By Eq. 13, a given mass lens lies along a particular contour in the space of Π vs. r_E (Figure 13). Armed with our event simulation code we have surveyed this Π vs. r_E phase space of

microlensing events for experiment sensitivity to microlensing parameters — with a particular emphasis on the lens mass. Table 1 gives a summary of the set of microlensing and astrometry parameters we considered in our Monte Carlo runs. We ran 500 instances of each parameter permutation given in the table — a total of 384 cases in all. In addition to the parameters specified in Table 1, in each of these experiments we assumed conditions similar to those described above in Figure 11: namely 3% photometry for event detection, and a 5-yr astrometric sequence starting at $t_{max} - t_0$, and sampling with uniform period $0.1\,t_0$. Microlensing parameter fits are made to the astrometric dataset combined with a 3% photometric dataset that spans the interval $t_{max} \pm 1$ yr. We considered fitting only the astrometry sequence in a few selected cases, but invariably found degraded parameter estimates (an illustrative example is given in Figure 14).

Figure 15 shows the variation of fractional lens mass error vs. astrometric error for three illustrative cases: $r_E = 100\ \mu$as, $\Pi = 50\ \mu$as ($m = 0.02\ M_\odot$); $r_E = 300\ \mu$as, $\Pi = 100\ \mu$as ($m = 0.1\ M_\odot$); and $r_E = 1000\ \mu$as, $\Pi = 200\ \mu$as ($m = 0.6\ M_\odot$). In each of these cases $p = 0.4$ and $t_0 = 0.1$ yr. Here the lens mass error is estimated from the observed uncertainties (residual sample standard deviations) in r_E and Π (and the generally non-zero covariance). This behavior is suggestive that the mass error scales by a power law of the astrometric error — we find these cases to be typical of the range of Monte Carlo cases considered.

Ignoring the correlation term, we can estimate the fractional mass error as a function of the fractional errors in r_E and Π from Eq. 13:

$$\frac{\widehat{\sigma_m}}{m} \approx \sqrt{\frac{4\sigma_{r_E}^2}{r_E^2} + \frac{\sigma_\Pi^2}{\Pi^2}} \approx \sigma_{ast}\sqrt{\frac{4}{r_E^2} + \frac{1}{\Pi^2}} \tag{14}$$

where the second equality comes from crudely estimating the uncertainties in r_E and Π by σ_{ast}. Figure 16 shows a scatter plot of the observed fractional mass error from all 384 of our Monte Carlo cases against the estimated fractional error given by Eq. 14. The agreement between the observed and estimated quantities is good, but we find Eq. 14 overestimates the fractional error at large values of σ_{ast}. A power-law fit to the data indicates that the observed error scales as the estimate in Eq. 14 (hence σ_{ast}) to the 0.8 power. We attribute this sub-linear scaling to the fact that astrometric fits supported by associated photometry resolve r_E and Π slightly better than the naive estimate of σ_{ast}. We attribute the observed scatter in the data to the correlation terms which are included in the observed error estimates, but are neglected in Eq. 14. We also note that the $t_0 = 0.2$ yr cases on average have lower observed σ_m/m and smaller scatter than the corresponding $t_0 = 0.1$ yr cases. This is not particularly surprising, as the slower time evolution allows for extended observation of the relative parallactic effects.

Finally, we have argued for and simulated differential astrometric experiments where we assume astrometry in a frame where the source is stationary. This reference frame must be established by observing field objects near the nominal source position. For LMC, SMC, and bulge events where there are many objects at small $\delta D/D$ with the source, the reference frame will absorb common parallactic motions. However, there will be residual frame drifts and rotations

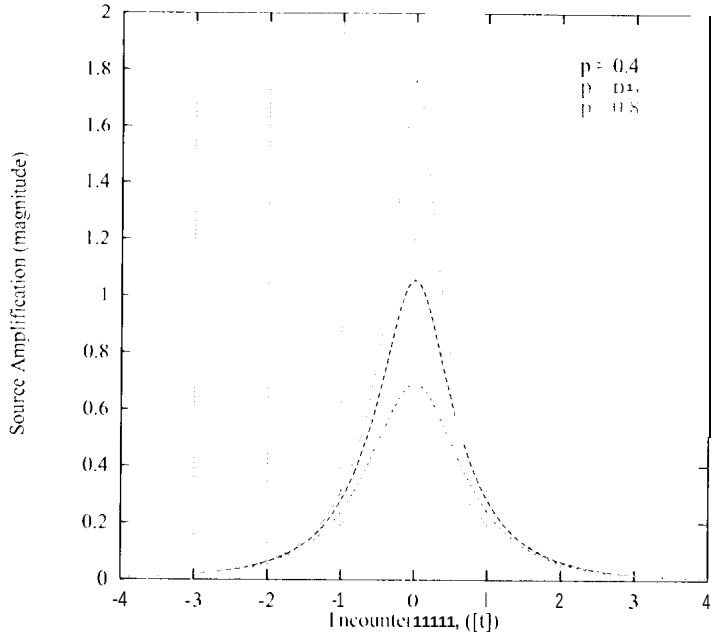

Fig. 5. Simple microlensing encounter lightcurves. This figure shows the expected lightcurves as a function of the normalized encounter time [t] for sample values of p from 0.2 (highest amplification) to 1 (lowest amplification).

r_E (μas)	H (μas)	p	t_0 (y')	σ_{ast} (μas)
100	50	0.4	0.1	5
300"	75	0.8	0.2	10
1000"	100			25
	200"			50
				75
				100"
				150
				200"

Table 1: Microlensing Monte Carlo Parameter Space. This table gives the set of microlensing and astrometric accuracy parameters we considered in our Monte Carlo runs. We ran a complete set of cases spanning all possible permutations of these parameter values (384 cases in all).

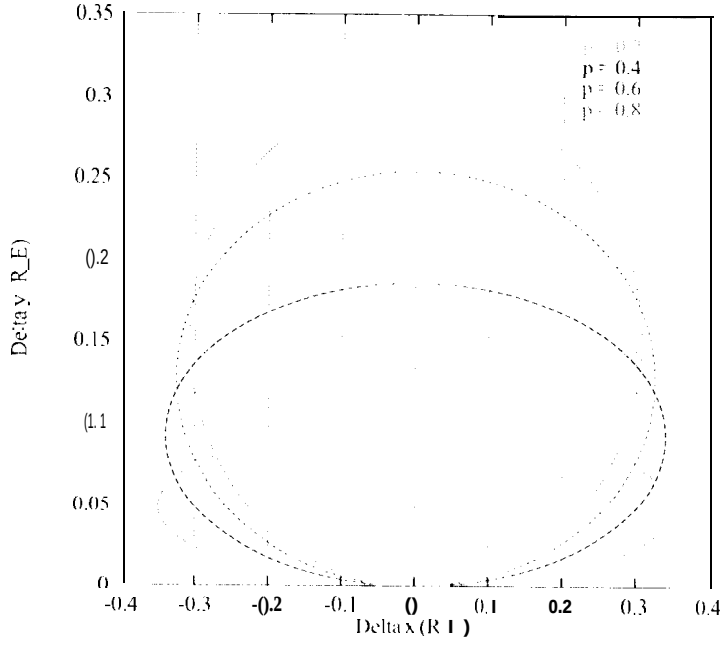

Fig. (i. Simple microlensing encounter center-of-light motion. Shown in red for our sample p-values are the motions of the apparent center-of-light position traces relative to the nominal source position for encounter times $-20 \leq [t] \leq 20$ (Eq. 9). The profiles are elliptical (note the anisotropy of the scale), and are seen to become more eccentric with decreasing p-value (Eq. 10).

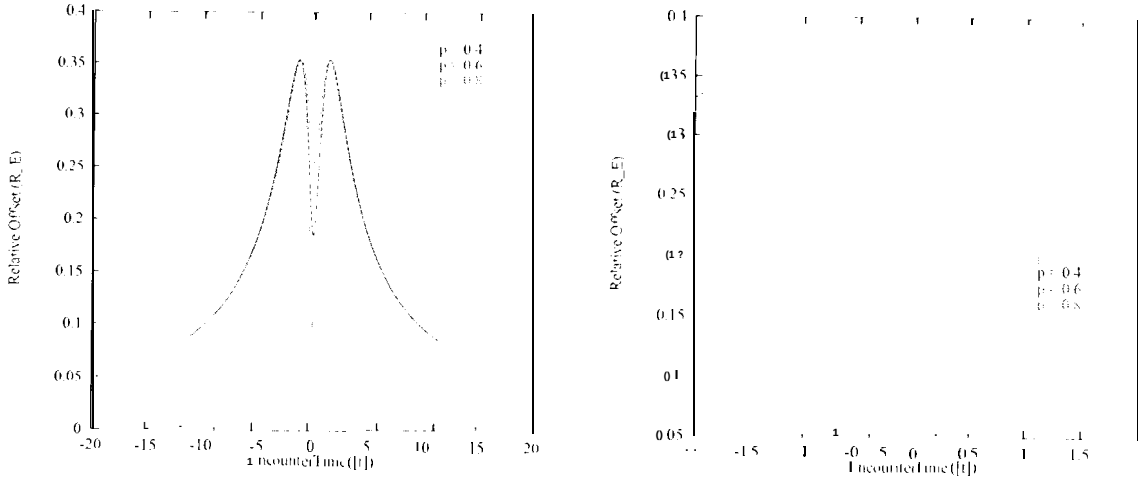

Fig. 7. Simple microlensing encounter apparent position perturbation magnitude. Left: the apparent source position shift *magnitude* in units of R_E as a function of the encounter time $-20 \leq [t] \leq 20$ for our example values of p. Right: the same quantity for $-2 \leq [t] \leq 2$. The dips in the perturbations are a ramification of the increasing eccentricity (Eq. 10) of the apparent source excursions with decreasing p as seen in Figure (i.

resulting from unknown velocity dispersion among the reference objects (and source). The residual linear frame drifts are large (mas yr^{-1}) on the scale of the microlensing astrometric excursion. The frame rotations will be small ($O(10^{-1})$ rad yr^{-1}), but to the extent that the source is not at the ("('111 er of the astrometric frame this too adds an effective linear drift to the differential frame of order 1 ()() μas yr^{-1}. So in practice the microlensing fit process must account for linear frame drifts that are large compared with the scale of the microlensing excursion. 1! is straightforward to extend the microlensing parameter model to include a frame drift. Figure 17 gives an example of allowing for a random drift in the astrometric frame, and using an extended microlensing model to solve for this quantity. The physical parameters of the microlensing event in Figure 17 are the same as those used in Figure 11: r_E = 300 μas, H = 100 μas, t_0 = ().1 yr; and we have taken 50 μas astrometry. To this we have added 1.5 mas yr^{-1} of frame drift in a random orientation to the lens motion. The microlensing fit does an acceptable job of identifying the frame drift, bolstered by the time base of astrometry at late encounter times (not shown in the figure). We do not find a coupling between frame drift and the quantities of interest in determining the lens mass: r_E and 11. We have added random frame (I rifts to several of the Monte Carlo cases described in Table 1, and find that such drifts do not significantly effect our simulation results. This is reasonable, as both r_E and 11 are estimated from the curvature of the astrometric path.

4. Summary and Discussion

We have specialized the Miyamota and Yoshi suggestion to measure the astrometry of the lensing event photocenter. We agree with their conclusions: that high-precision astrometric observation of MACHO microlensing events hold the promise of determining fundamental lens parameters (mass, proper motion, transverse velocity) in a model-independent fashion. We maintain that it is sufficient to measure the motion of the center-of-light. In particular, accurate differential astrometry is sufficient obtain the lens mass without additional assumptions, and reasonable lens distance and transverse velocity ('st in iiit es ("iiii 1)(' obtained from an independent model of source (listance and proper motion. Alternatively, wide-angle astrometry can simultaneously determine the S0111'("(" and lens kinematic parameters, and again the lens mass. Clearly the potential for probing the physical parameters of the halo object population by astrometric techniques is enormous.

A program to probe microlensing events photometrically detected in the galactic bulge seems plausible for the planned Keck Interferometer (1{1). J{] requires a bright guide star to track atmospheric fluctuations of the interferometric fringes. The brightest bulge objects are 1 6th magnitude, within the fringe tracking capabilities for the two]() mapertures. The expected 10 μas astrometric performance of KI yields microlensing parameter estimates sufficient to constrain lens parameters for individual events, which will give profound insight into the nature of these objects.

However, events in the LMC or SMC are not detectable from the Keck site, both because of geography and sensitivity. The brightest objects in the LMC are 17 18 magnitude, arguably

fainter than the tracking capabilities of the 1{1. However, the declination of these fields would require KI zenith angles that severely degrade the astrometric performance. A large aperture astrometric interferometer in the Southern hemisphere such as the VLT interferometer (VLTI 1 Beckers et al 1990) could measure Magellenic cloud events. Such measurements are compelling because they would preferentially probe the population of galactic halo objects.

A number of authors have suggested the application of planned space-based global astrometric techniques to analyze these events (Høg et al 1995, Miyamoto & Yoshi 1 995). In space-based applications astrometric references can D(' drawn from a global astrometric frame tied to extragalactic objects, and the positions, proper motions, and parallaxes Of t 11(',S(' references are known to a few microarcseconds. Thus the necessity of establishing a narrow-angle relative frame for differential astrometry is removed. Further, astrometry at late times establishes the source proper motion and parallax in the global frame thereby establishing the source motion and distance. With the source distance and kinematics established, the lens parameters are all uniquely determined. Assuming ground-based observations measure lens masses in the manner we describe, we believe the role of space-based microlensing astrometry programs by planned astrometric space missions such as SIM (Unwin et al 1997) and GAIA (Lindegren et al 1995) will be in probing the positions and kinematics of the lens objects.

Finally, in the near future it is possible that CCD-based astrometry could make detections of microlensing astrometric perturbations, and possibly make rough estimates of lensing parameters, and/or breaking some of the degeneracies in photometric microlensing observations (see below). Pravdo and Shaklan (Pravdo & Shaklan 1 996) report night-to-night astrometric repeatability of 200 μas in data taken at the Palomar 5 m telescope, and speculate that limits might approach 10[) μas at the 10 m Keck Telescope. In further assessing these prospects we anxiously await the results of two nights of Keck observations recently made by Pravdo and Shaklan (Shaklan 1997).

One of the key assumptions we have made in this work is the assumption of a dark lens. This assumption is reasonable given the success photometric programs have had in fitting (lark lens amplification models to photometric data. However, the instance of a luminous lens is possible and interesting (Miralda-Escudé 1996, Paczyński 1996b), and the astrometric model derived here can be augmented in a straightforward way. One operational question that arises is how does one determine whether a dark lens model is appropriate for a given microlensing event. While one could straightforwardly test the luminous lens hypothesis by adding a relative source/lens luminosity parameter to the microlensing fit model presented here, a more obvious and compelling resolution to this question is contained in the possible chromaticity of the observables. If the lens is luminous, then its spectral content is in general different from that of the source implying that both the photometric and astrometric observables will be functions of wavelength. Making the observations in a variety of spectral bands will identify the relative source-lens intensity and color, and provide the necessary data to robustly extend the microlensing model to the case of luminous lenses. We defer the quantitative analysis of the luminous lens case to future work.

The closely related problem of image blending is discussed in recent work by Alard (Alard 1996), and Woźniak & Paczyński (Woźniak & Paczyński 1997), who consider the possibility that a second source (possibly unrelated to either source or lens) is unresolved from the image. Woźniak & Paczyński find that the degeneracies in photometric observation of such events result in systematic errors in estimating lensing parameters. We concur with the speculation put forward by Woźniak & Paczyński that multi-spectral astrometry and photometry breaks the degeneracy in (some subset of) blended events, and point this out as a particularly important case for future Study.

A second minor operational difficulty in the analysis presented here is that interferometric astrometry does not measure the center of light as calculated in Eq. 7, instead it measures the average sky position of fringes from the lensing images. In the case where the images are partially resolved by the interferometer the two quantities can be different. To set the scale of the problem we note that astrometric interferometers such as the Palomar Testbed Interferometer and the planned Keck Interferometer have baselines on the order of 100 m, and (will) operate astrometrically at K-band ($\lambda = 2.2\ \mu$m), thus have a fringe spacing $\lambda/B \sim 5$ mas on the sky. Near maximum amplification (when image 2 is significant) if the image separation ($\approx 2r_E$) is comparable to the fringe spacing there is an observational correction to Eq. 7 (strictly speaking, this case no longer satisfies the resolution conditions of microlensing). For the range of lens parameters considered here this correction is insignificant, but can become important for larger values of r_E: namely more massive and/or closer lenses.

Astrometric Detections - Non-MACHO Events A number of authors have suggested to broaden the applicability of the astrometric techniques to non-MACHO microlensing events (Miralda-Escudé 1996, Paczyński 1996b). These events could potentially be detected astrometrically in programs that concentrated on high proper motion objects (so as to sweep-out larger solid angles), or as a part of broader companion search program (something we have integrated into our PTI program). While much of the phenomenology we have developed in §2 is directly applicable, there are a couple of practical difficulties in establishing lensing parameters in such events measured differentially. The first is the absence of a ready supply of reference objects that share common parallactic motions as the source. The fact that the rich LMC, SMC, and bulge fields used in the photometric surveys naturally yield an abundance of reference objects for which $\delta D/D$ is small makes events in these fields unique. We speculate that without that common parallactic reference, the systematic errors in the determination of $\mathbf{l}$ will be too large to establish a precise lens mass. The second practical difficulty would be the absence of accompanying photometry in this more general class of microlensing events. We observe that simultaneous photometry does much to constrain the time scale of the event, making the job of interpreting the astrometry considerably easier (see Figure 14 and similar remarks in Høg et al 1995). In astrometrically detected events, by the time it is clear that an astrometric sequence is a microlensing candidate, most (if not all) of the photometric effects have passed.

Complex Lenses While the majority of photometrically detected events are consistent with single lens hypothesis, a number of binary lens events have been reported (Udalski et al 1994. Alard et al 1995a, Bennett et al 1996). In a recent preprint Dominik (Dominik 1997) argues that photometry alone does not uniquely constrain the binary lens parameters. We speculate that additional astrometric information would break the degeneracies among various hypotheses in binary lens events through straightforward extensions of the astrometric theory developed here. We defer the analysis of the binary lens case to future work.

The work described in this paper was performed at the Jet Propulsion Laboratory, California Institute of Technology under contract with the National Aeronautics and Space Administration.

REFERENCES

Alard, C., Mao, S., Guibert, .1. 1995, A&A 300, 17 (astro-ph/9506101).

Alard, C. et al (the DUO collaboration) 1995, Msngr N), 31.

Alard, C. 1996, A&A in press (astro-ph/9609165).

Alcock, C. et al (the MACHO collaboration) 1995, ApJ 454, 1,125 (astro-ph/95061 14).

Alcock, C. (It al (the MACHO collaboration) 1996. ApJ submitted (astro-ph/9606165).

Beckers, J.M. et al 1990, Proc. SPIE 1236, 108.

Bennet 1, D.P. et al (the MACHO collaboration) 1996, Nucl. Phys. 1'1'()(". Suppl.51B.152 (astro-ph/9606012).

Buchalter, A. and Kamionkowski. M. 1996, ApJ 469, 676 (astro-ph/ 9604144).

Colavita. M.M. et al 1994, Proc. SPIE 2200,"89.

Dominik. M. 1997, preprint (astro- ph/ 9703003).

Gaudi, B., and Gould, A. 1997, ApJ 477, 152 (astro-ph/9601030).

Gould, A. 1992, ApJ 392, 442.

Gould, A. 1996, PASP 108, 46 5G (astro-ph/ 9604014).

Hog, E., Novikov, 1.1)., and Polnarev, A.G. 1995, A(QA 294, 287.

Lindegren, 1,., Perryman, M. A., and Loiseau, S. 1995, Proc. SPIE 2.477, 91.

Miyamoto, M. and Yoshi, Y. 1995, AJ 110, 1427.

Miralda-Escudé, ,1.1996, ApJ 470, 1,113 (astro-ph/9605138).

Paczyński, B. 1986a, ApJ 301, 503.

Paczyński, B. 1986b, ApJ 304, 1.

Paczyński, B. et al (the OGLE collaboration) 1995, BAAS 187, # 14.07

Paczyński, B. 1996a, ARA&A 34, in press (astro-ph/9604011).

Paczyński, B. 1996b, Acts Ast. submitted (astro-ph/9606060).

Pravdo, S.H. and Shaklan, S.B. 1996, ApJ 465, 264.

Refsdal, S. 1964, MNRAS 128, 295.

Renault, C. et al (the EROS collaboration) 1996, A&A in press (astro-ph/9612102).

Shaklan, S.B. 1997, private communication.

Udalski, A. et al (the OGLE collaboration) 1994, ApJ 436, L103 (astro-ph/9407084).

Unwin, S., Boden, A., and Shao, M. 1997, Proc. STAIF, All' Conf. Proc. 387, 63.

Woźniak, P. and Paczyński, B. 1997, preprint (astro-ph/9702194).

This preprint was prepared with the AAS LaTeX macros v4.0.

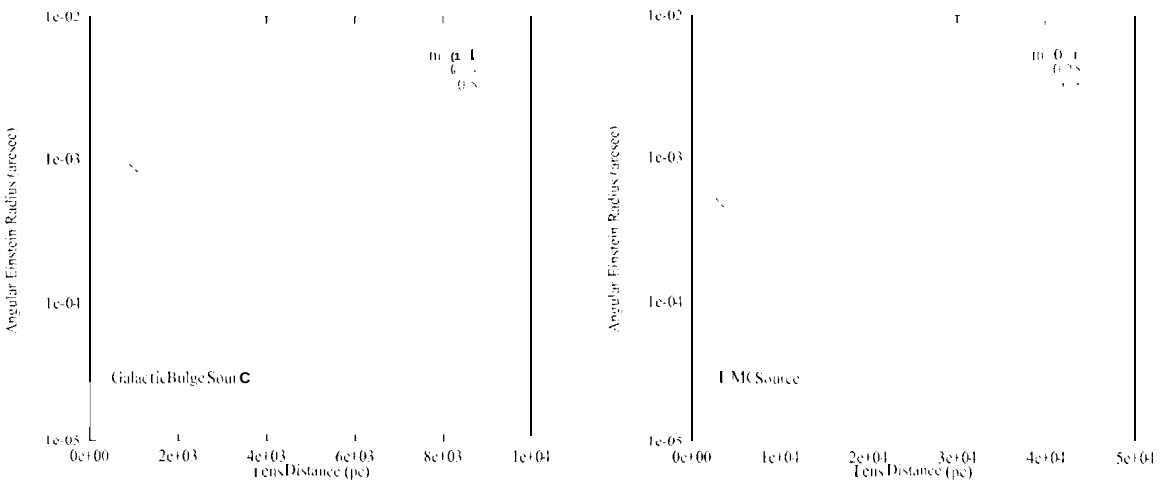

Fig. 8. Microlensing Encounter Angular Einstein Radius. Left: the angular Einstein radius (r_E) for 1)111$(' sources as a function of lens distance for lens masses between 0.05 and 1 $M_\odot$ (m = 0.05, 0.1, 0.25, 0.5, 1 $M_\odot$). Right: the same quantity for LMC events. The astrometric signature magnitude for microlensing events is given by $2^{3/2} r_E \approx 0.35\, r_E$. Thus a m = 0.1 $M_\odot$ object at 8 kpc lensing a LMC source has an angular Einstein radius of 300 μas and a maximum astrometric signature of roughly 100" μas.

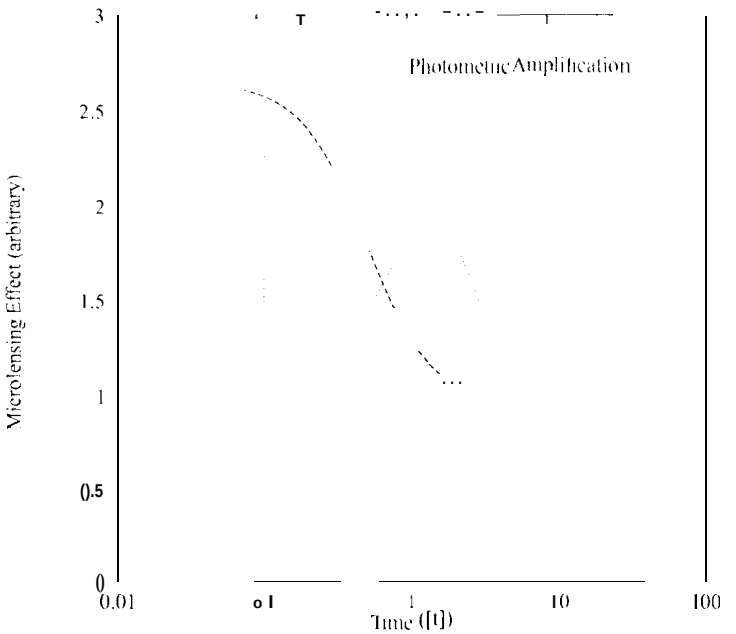

Fig. 9.- Comparison of Microlensing Astrometric and Photometric Effects. This figure shows the amplification factor and magnitude of the astrometric perturbation as a function of encounter time for an event with $p = 0.4$. The 1)11010111('I ric amplification is seen to decay from maximum amplification to a nominal value of 1 (no amplification) in roughly **1** event **t** ime scale (t_0). By comparison, t he astrometric perturbation (normalized t 0 t he perturbation at f □ t_{max} , $r_E p/(p^2$ -i **2))** increases to its maximum value at $[t] \sim$ **1,** and **t** hen decays t 0 zero in **a t** ime scale several orders **of** magnitude larger **t** han the photometric amplification. If $t_0 \sim 1$ month as reported for L MC microlensing events by t he MACHO collaboration, measurable astrometric deflections in such events would last over periods of years depending on astrometric sensitivity.

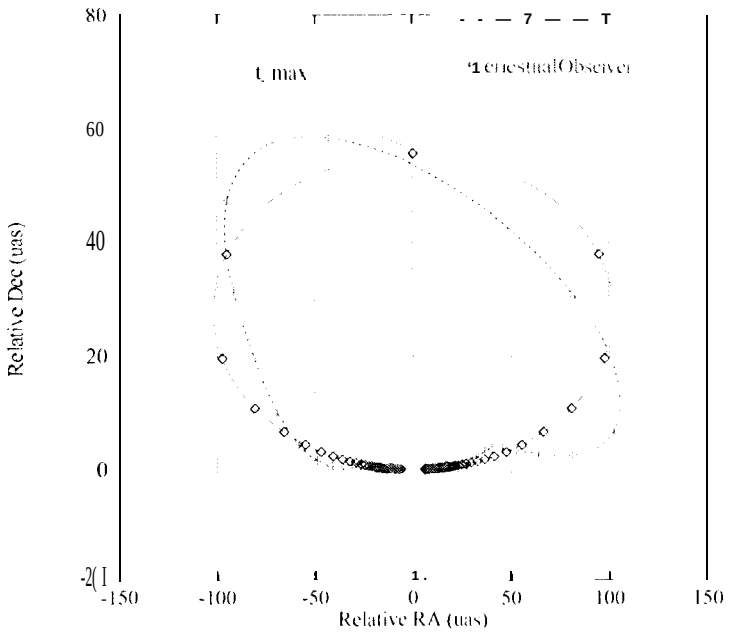

Fig. 10. Parallactic Perturbation to Barycentric Microlensing Astrometry. This figure shows the astrometric deflection for a $p = 0.4$ microlensing event as viewed by barycentric and terrestrial observers over a period of $\pm 50\ t_0 = \pm 5$ yr. Marks on the two trajectories are given at $t_0 = 0.1$ yr intervals. (The parallactic motion of the background source – 20 μas – is removed to facilitate comparison.) The background source is taken in the LMC ($D_{so} \sim 50$ kpc), and the lens is taken to be in the galactic halo ($D_{lo} \sim 8$ kpc), with an angular Einstein radius of 300 μas ($m \sim 0.1\ M_{\odot}$). Astrometry sufficient to measure the microlensing perturbation will also measure the parallax effects. A parallax measurement can be used to estimate the relative source/lens distance to the lens, which in turn allows the lens mass and relative transverse velocity to be inferred for individual events. The time marks corresponding to (barycentric) t_{max} are shown.

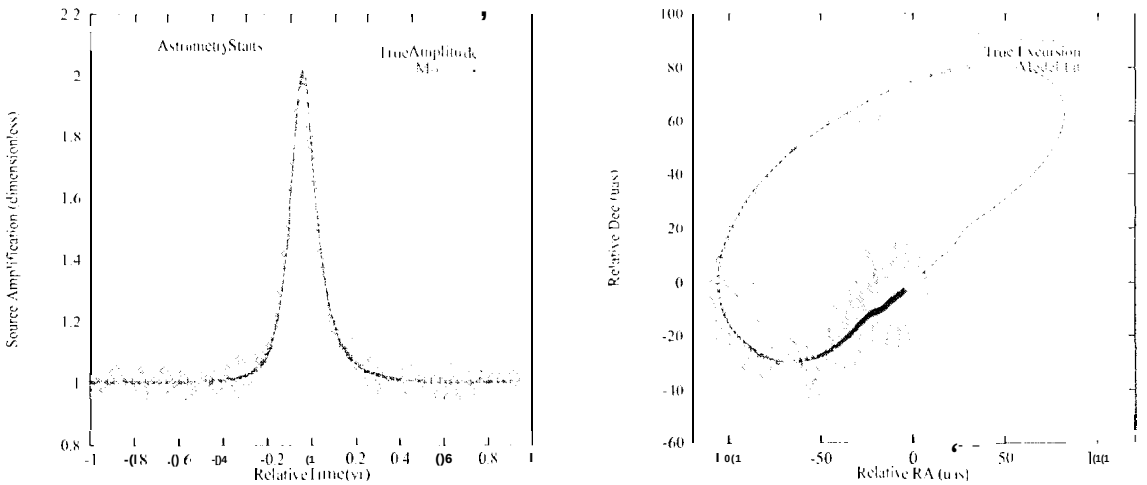

Fig. 11. Sample Microlensing Model Fitting. Here we show an example instance of fitting a microlensing model to synthetic terrestrial photometry and astrometry datasets for a microlensing encounter. The critical parameters for the event are a lens motion position angle of 30 deg, p = 0.4, r_E = 300 μas, and $H_\square$100" μas (m = 0.1 $M_\odot$). We assume the event is identified photometrically, and differential astrometric measurements commence after that detection. The microlensing model described in §2 was simultaneously fit to both the photometric and astrometric data. Shown in each are the simulated data, true values, and the model fit. Left: the photometric lightcurve results. In this example we assume 3% photometry error. The time units on the x-axis are plotted relative to the barycentric t_{max}. Once a microlensing interpretation seems likely, we commence astrometric measurement this time point is shown. Note that the time of maximum amplification for the terrestrial observer is offset relative to a barycentric observer. Further, the lightcurve is slightly asymmetric with respect to the time of maximum amplification. Both of these effects are well known for terrestrial microlensing observation. Right: the corresponding depiction for the astrometry sequence relative to the nominal source position. The simulated 10 μas astrometric measurements begin shortly before maximum magnification, and continue for 50 t_0 after maximum magnification. The true excursion trajectory is shown over the complete excursion, but the microlensing model fit prediction is rendered only for the interval of the astrometric measurements.

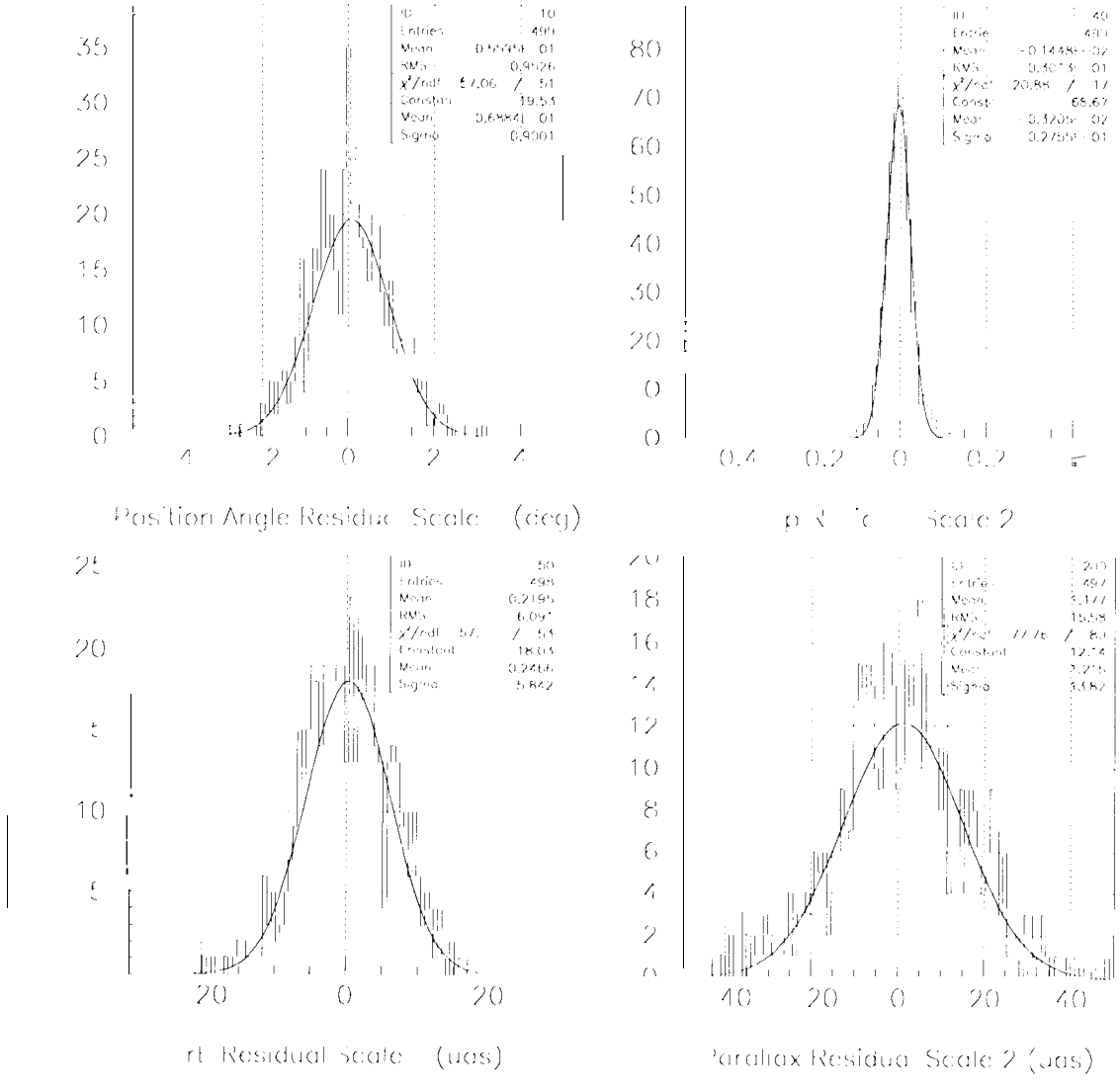

Fig. 12. Sample Monte Carlo Fit Residual Distributions. Here we show a sample of the microlensing model fit residual distributions obtained in 500 measurement sequence instances taken from the microlensing event depicted in Figure 11. Measurement parameters are the same as discussed in Figure 8: 3% photometry and 10 μas differential astrometry. Distributions are shown for lens motion position angle (top left), normalized impact parameter (top right), angular Einstein radius (lower left), and relative parallax (lower right). These astrometric experiments are seen to yield fractional uncertainties in the angular Einstein radius and parallax of 2% and 16%, respectively, yielding a 16% error in the lens mass estimate by Eq. 13.

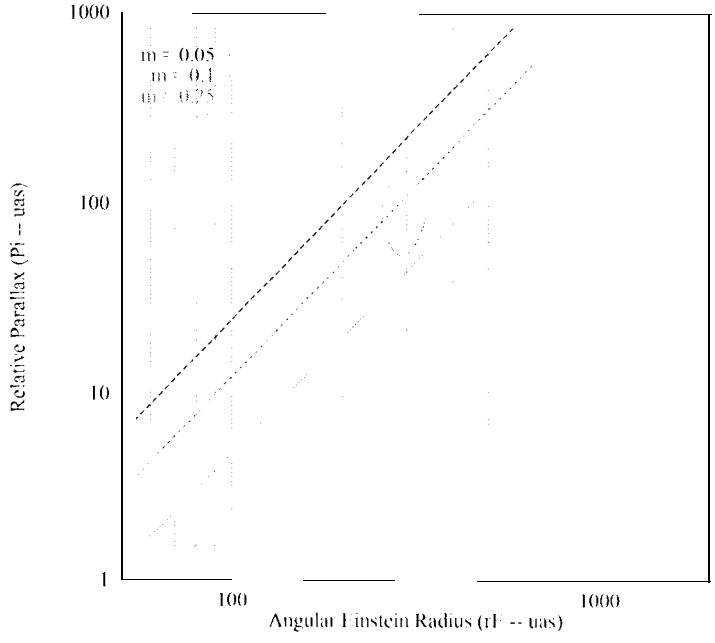

Fig. 13. Contours of Constant Mass in Π vs. r_E. After Eq. 13, a given lens mass constrains the values of r_E and Π to lie along a particular contour. The problem of estimating the lens mass may be envisioned as simultaneously estimating Π and r_E from astrometry of the microlensing excursion. For a given event, astrometry of finite accuracy defines an uncertainty region. For the event depicted in Figure 11 ($r_E = 300\ \mu$as, $\Pi = 100\ \mu$as, $m = 0.1\ M_\odot$) a presumed covariance ellipse is shown ($\sigma_{r_E} = 40\ \mu$as, $\sigma_\Pi = 50\ \mu$as, with a correlation coefficient of -0.5, roughly corresponding to results obtained with $\sigma_{ast} = 50\ \mu$as) in this space that defines the range of possible lens masses.

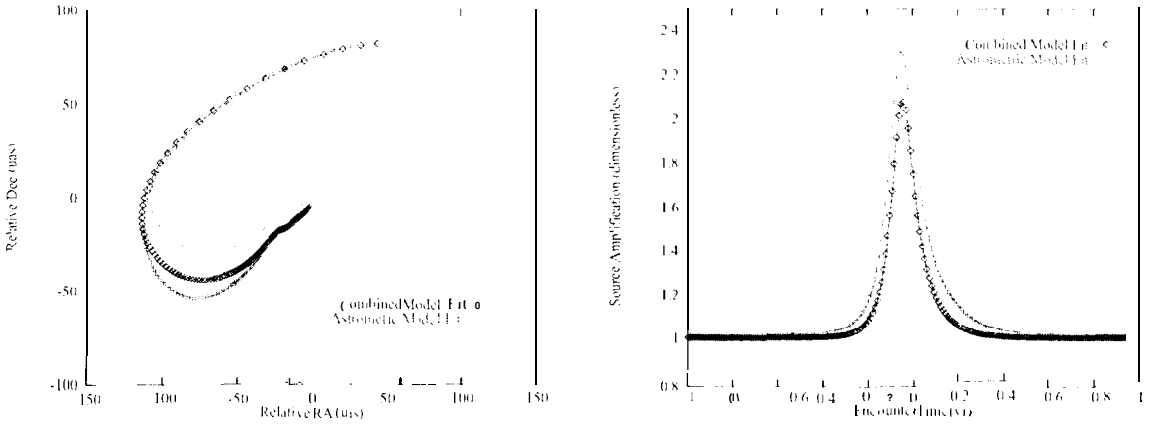

Fig. 14.- Microlensing Combined Model Fitting. Here we depict the utility of fitting a microlensing model to combined photometry and astrometry datasets vs. fitting the astrometric set only. The physical parameters for the event are the same as in Figure 11: a position angle Of 30 deg, $p = 0.4$, $r_E = 300$ μas, $H = 100$ μas, and we have assumed 75 μas astrometry in this instance. Top Left: Renderings Of the true astrometric excursion and model fits using both photometric and astrometric datasets (combined), and the astrometric dataset only. By definition the astrometric-only fit matches the astrometric dataset (not shown for clarity) better than the combined fit. Top Right: The photometric predictions from the same two model fits at left, compared with the true photometry. Clearly the combined fit model matches the photometric data better than the fit model where the photometry is ignored Or unavailable. Bottom Left: a relative parallax fit residual histogram for 500" instances Of the experiment depicted above using the combined datasets in the fit metric. Bottom Right: the same quantity using the only the astrometric data in the fit metric. Clearly utilizing the photometric data greatly constrains the error of the parallax measurement (the dominant error in the lens mass estimate) by almost a factor of two.

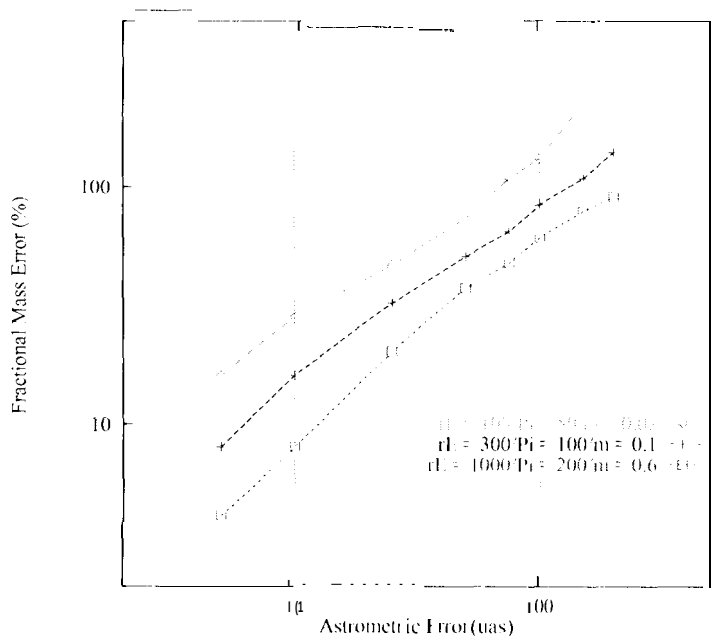

Fig. 15. Fractional Mass Error vs. Astrometric Error: 'T'1ll'('(' Examples. I1('1 '(! we Snow" three samples of fractional mass error vs. astrometric error from our ensemble of Monte Carlo results. The three examples are: τ_E = 100" μas, 11 = 50 μas (m = ().()2 $M_\odot$); τ_E = 300 μas, 11 = 100" μas (7// = 0.1 $M_\odot$); and 7"„ = 1000 μas, 11 = 200" μas (7// = 0.6 $M_\odot$). Not surprisingly, we find the fractional mass error to scale as a power law of the astrometric error in all our Monte Carlo results.

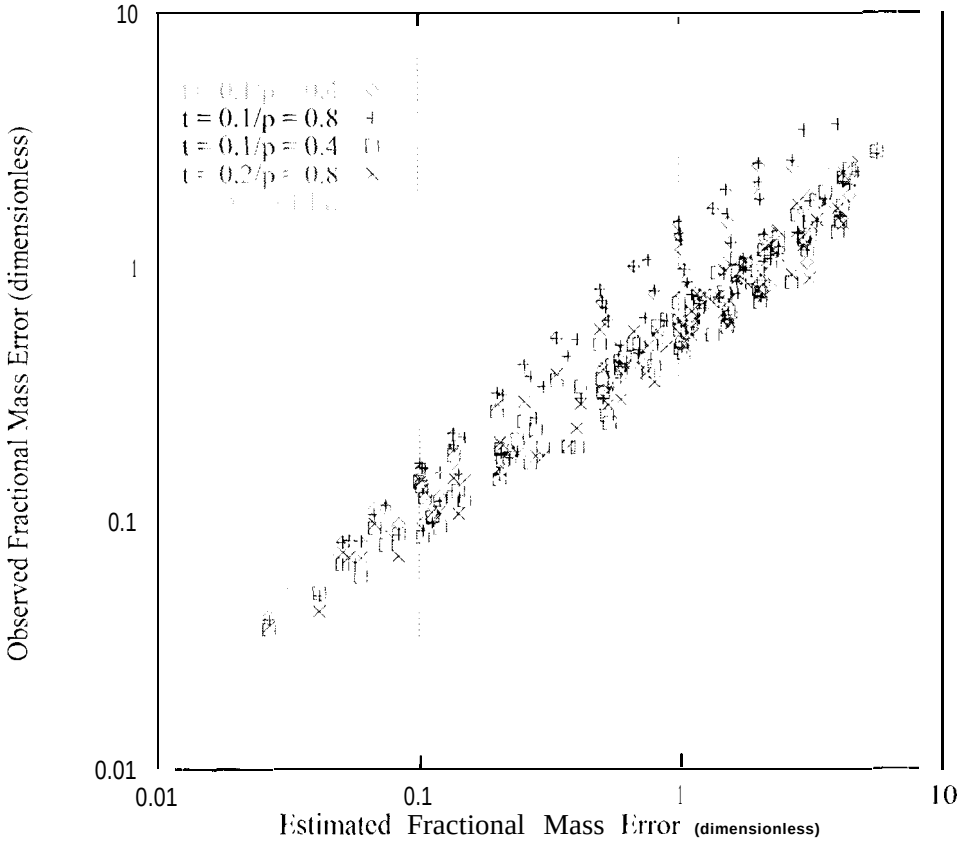

Fig. 16. Scatter of Observed Mass Error vs. Estimated Mass Error. 11('1'(' we show the scatter of the observed fractional mass error vs. the estimated fractional mass error given in Eq. 14. Each data point represents the fractional mass error obtained in 500" instances of measurement sequence fitting. Data sets for t_0 = ().1 yr, ().2 yr and p = 0.4, 0.8 are shown separately the intrinsic scatter in the t_0 = ().2 yr results is noticeably smaller. The data are seen t 0 correlate reasonably well with the crude mass estimate of Eq. 14, but it overestimates the mass error at larger values. A simple parametric fit shows the observed fractional mass error to scale (with moderate scatter) to the estimated fractional mass error to the 0.8 power. We attribute the scatter in the data to the correlation in errors included in the observed error calculation but explicitly ignored in Eq. 14.

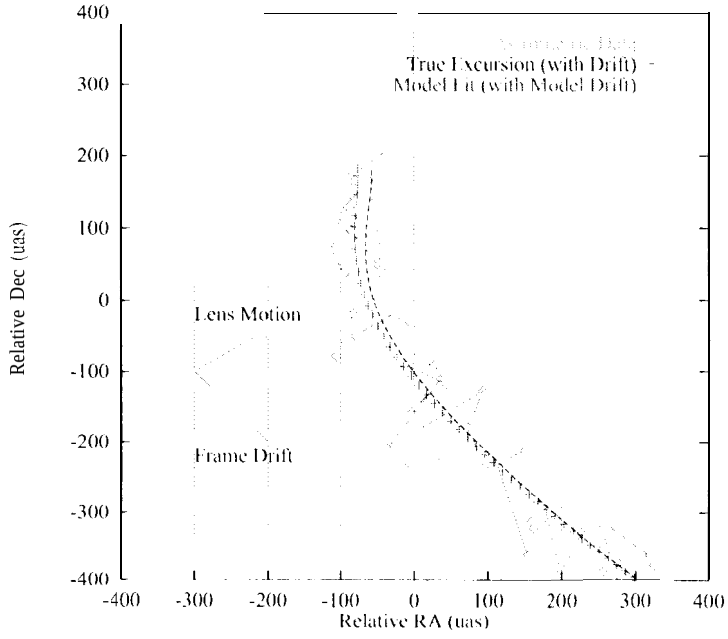

Fig. 17. Microlensing Astrometric Fit With Frame Drift. Shown is the result of an astrometric experiment where we have added a linear drift into the differential astrometric frame. The microlensing parameters of this event are the same as used in Figure 11: r_E = 300 μas, H = 100 μas, t_0 = 0.1 yr; and we have taken 50 μas astrometry. We added 1.5 mas yr^{-1} of frame drift in a random orientation to the lens motion (vectors indicating the frame drift and lens motion direction are shown). The microlensing fit does an acceptable job of identifying the frame drift. We do not find a coupling between frame drift and the quantities of interest in determining the lens mass: r_E and H. We have added random frame drifts to several of the Monte Carlo cases described in Table 1, and find that such drifts do not effect our simulation results.